JOURNAL OF MATERIALS SCIENCE **39** (2004) 6951–6956

Investigation of fatigue cracks in aluminium alloys 2024 and 6013 in laboratory air and corrosive environment

CH. ZAMPONI, ST. SONNEBERGER, M. HAAKS, I. MÜLLER, T. STAAB
Helmholtz-Institut für Strahlen- und Kernphysik der Universität Bonn, Nußallee 14-16, D-53115 Bonn, Germany
E-mail: zamponi@iskp.uni-bonn.de

G. TEMPUS
Airbus Deutschland, Hünefeldstrasse 1-5, D-28199 Bremen, Germany

K. MAIER
Helmholtz-Institut für Strahlen- und Kernphysik der Universität Bonn, Nußallee 14-16, D-53115 Bonn, Germany

Fatigue cracks have been generated in the commercial aluminium alloys AA2024 and AA6013 and analysed with a positron microprobe. This instrument provides laterally resolved positron annihilation measurements, which are sensitive to lattice defects like vacancies and dislocations. These commercial alloys have undergone a solution heat treatment and quenching prior to fatigue testing. Subsequently, they have been aged at room temperature and 190°C for AA2024 and AA6013, respectively. We performed the fatigue crack generation both in air and under the influence of a chemically aggressive environment (artificial seawater). Due to the corrosive environment hydrogen is probably produced at the fresh fractured surface in the vicinity of the crack tip. We discuss the possible implications of in-diffused hydrogen on the produced lattice defects, especially when there is a delayed migration of vacancies in the lattice, due to a reduced mobility.

1. Introduction

Age hardening in aluminium was discovered by chance in 1906 [1]. This effect was indispensable for the application of the lightweight metal aluminium for aircraft structures. Until a couple of years ago mainly the standard skin sheet alloy AA2024 (AlCuMg) was used for joining of fuselage structures by riveting or bonding. Since the advanced Laser Beam Welding (LBW) joining technique results in higher weight and cost savings than riveting or bonding, two years ago the first LBW fuselage shells were implemented in the Airbus aircraft A318. For realization of such LBW structures, weldable Al alloys have to be used. However alloy AA2024 is non-weldable. One suitable choice for LBW is the alloy AA6013, which has similar mechanical properties to AA2024 under laboratory conditions.

The potential for weight reduction depends strongly on the fatigue behaviour of the alloy AA6013, since fuselage structures undergo a dynamic loading. The crack growth rate is of particular interest in respect to both the safety and the inspection intervals of the component affected. In practice, effects of corrosion are superimposed onto those induced by dynamic mechanical stress. If stress corrosion cracking occurs, the crack growth rate can be considered to be the sum of crack propagation rate under inert conditions and crack growth due to stress corrosion cracking in that part of the cycle in which the threshold value of stress corrosion cracking is exceeded [2].

Both alloys, AA6013 and AA2024, show an environmental sensitive fatigue crack growth behaviour depending on the cyclic stress intensity factor ΔK and the frequency: decreasing the frequency from 40 Hz to 0.33×10^{-3} Hz 3.5% NaCl solution increases the fatigue crack growth rate compared to laboratory air. It passes through a maximum at a frequency of 1 Hz. For lower frequencies ($\leq$0.040 Hz), corresponding to more real in-service load conditions, the crack growth rate decreases to the level of laboratory air. This effect is clearly more pronounced for AA6013 than for AA2024 [3–6].

In order to improve the fundamental understanding of this environment-assisted fatigue crack growth behaviour, the plastic zone in front of fatigue cracks in both alloys generated in air and in a corrosive medium were examined.

Generally, size and geometry of the cyclic plastic zone give hints to the crack propagation behaviour [7], since plasticity is microscopically determined by the behaviour of dislocations and atomic defects like

vacancies. Positron Annihilation Spectroscopy (PAS) is a highly sensitive method for the detection of these defects in solid matter [8, 9]. We performed a series of laterally resolved positron annihilation measurements of the plastic zone for the aluminium alloys AA2024 and AA6013 in air and in corrosive conditions. These investigations were done employing the microbean provided by the Bonn Positron Microprobe (BPM) [10, 15].

PAS is not directly sensitive for dislocations. As dislocations are shallow traps for positrons at room temperature (RT), they are observed by the associated non-equilibrium vacancies generated by plastic deformation. Since the migration enthalpy of vacancies in aluminium is 0.61 ± 0.03 eV [11], these vacancies are mobile at RT. Here the plastic zone is defined as the zone of increased vacancy density in front of the crack tip.

2. Experimental

Sheet samples (1.6 mm thick) of the alloy AA2024 T351 (AlMg1.6Cu4.4) have been used as manufactured. This means a solid solution heat treatment at 490°C followed by quenching to room temperature had been performed. The naturally aged condition is reached by storing the sheets at RT for more than four days.

Samples (1.6 mm thick sheets) of the alloy AA6013 T6 (AlMg1Si0.8Cu0.9) were used in the artificially aged condition (190°C, 4–5 h), after a solid solution heat treatment at 560°C followed by quenching to RT. As described above, both alloys undergo a precipitation heat treatment resulting in formation of coherent (AA2024) or semi-coherent (AA6013) precipitates [12, 13].

Due to the fixed thickness of the sheets, a scaled down CT (Compact Tension) geometry is used under plane strain conditions for all fatigue crack samples. The dimensions of all samples are 30 mm × 31 mm × 1.6 mm. The deformation process was stopped at a crack length of 10.5 mm corresponding to a ΔK of 15 MPa$\sqrt{\text{m}}$ at the crack tip.

A deformation apparatus operating with a piezo ceramic actuator was used for crack production [14]. This setup also provides the possibility to operate under corrosive conditions. The device provides an elongation range of 150 microns and crack propagation takes place in the strain control regime. The load limits were adjusted to 500 N resp. 50 N. All samples were deformed using a frequency of 1 Hz. As corrosive environment a 3.5% NaCl solution with 0.2% $Na_2Cr_2O_7$ and 0.2% Na_2CrO_4 as corrosion inhibitors was used.

All positron measurements have been performed by the BPM [10, 15] due to the expected size of the plastic zone in the micron range. The crack tip was scanned using a beam diameter of 20 microns and a grid size of 50 microns. The positron beam energy of 30 keV equals a mean implantation depth of 4 microns. Therefore, surface effects can be neglected.

Positrons are sensitive mobile probes to detect defects in solids, like vacancies or dislocations, both having an open volume which is an attractive potential for positrons. After a short period of thermalisation of about 3 ps the positron diffuses through the lattice and annihilates with an electron. In the laboratory system the momentum of the annihilating particles leads to a Doppler shift of the 511 keV peak line of the emitted gamma rays. Due to the low thermal energy of the positron (≈40 meV at RT) the momentum of the positron can be neglected compared to the momentum of the electron. In open volume defects the average momentum of electrons is lower than in the bulk. Hence, the Doppler broadening of the 511 keV photo peak reflects the defect density in the observed area. The change of the line shape of the peak is usually characterised by the integral line shape parameter. This S-parameter is defined as the integral over the central part of the peak divided by the total area under the photo-peak. For a detailed review of positron annihilation spectroscopy see: [16, 17]. In this context an increased S-parameter indicates an increased density of dislocations or other open volume defects.

For comparison, all S-parameters of different samples (alloys AA2024, AA6013) are normalised to the bulk S-parameter of pure (99.999%) Al annealed at 500°C for 4 h in high vacuum (S/S_{Al}). The energy spectrum of the annihilation radiation is measured by an intrinsic Ge-detector with an energy resolution of 1.2 keV at 478 keV (^{7}Be).

To investigate the influence of annealing behaviour at RT in the plastic zone over a long time scale, the spatially resolved measurements at the crack tips are repeated after several weeks.

3. Results

3.1. PAS values in the undeformed alloys

In bulk Al-alloys positron trapping occurs exclusively at precipitates if their positron affinity [18] is higher than that of the surrounding matrix [19–21]. This is the case for the alloys considered here. The bulk S-parameter is determined by two effects: the valence electron density and the chemical environment of the positron trapping site. Firstly, in the case of semi-coherent precipitates, which exhibit misfit dislocations or open volume defects at some interfaces towards the Al-matrix, positrons are trapped at the non-coherent interfaces leading to a higher S-parameter. Secondly, the momentum of the core electrons depends on the atomic number of the alloyed elements so that the chemical composition of the precipitates also influences the S-parameter e.g. pure Cu has a much lower S compared to pure RC.

In AA2024 the effect of the dislocations (increased S) is cancelled out by the high concentration of Cu in the precipitates (see Table I), while in AA6013 the precipitates consist of MgSi (β') or AlMgSiCu (Q′) which cause a chemical shift to a higher S-parameter than in pure aluminium.

TABLE I Bulk value of S/S_{Al} in the two different Al-alloys

Alloy	AA 2024	AA 6013
$S_{\text{bulk}}/S_{\text{Al}}$	1.001	1.025

3.2. Plastic zone AA2024 deformed in air

Fig. 1 shows a contour plot of the plastically deformed region in front of a crack tip in AA2024 deformed in air. In all following contour plots the origin of the coordinate system is set to the position of the crack tip. The crack direction is parallel to the x-axis. The total amount of annihilation events collected for each point is 3×10^5, which corresponds to a statistical error $\Delta S/S = 2 \times 10^{-3}$. The dimension of the plastic zone is 125 μm $\times$ 175 μm and a maximum value of S/S_{Al} equal to 1.017 ± 0.002 is observed at the crack tip. The extension of the plastic zone is given by a significant increase of the S-parameter. In AA2024 this limit is set at $S/S_{\mathrm{Al}} = 1.006$. The size of the plastic zone in AA2024 created in air does not change in the course of several weeks.

Fig. 2 shows a line scan at $x = 50$ μm as an example for the statistical error distribution. The solid line is a guide for the eye.

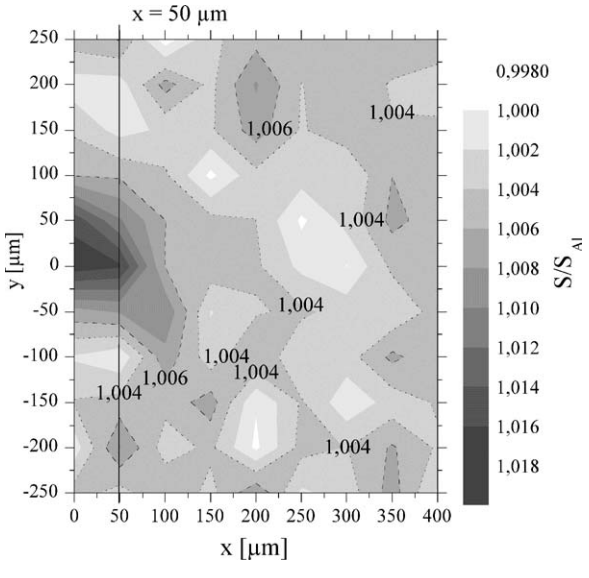

Figure 1 Plastic zone in front of a crack tip in AA2024 deformed in air. The image shows an area of 400 $\times$ 500 μm. The greyscale shows the S-parameter relatively to well annealed high purity Al. The solid line shows the position of the line scan in Fig. 2.

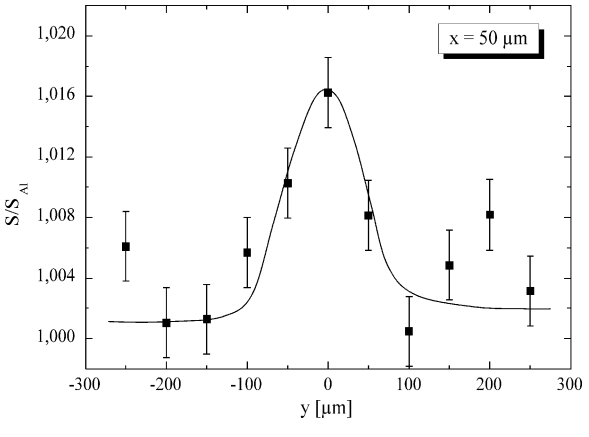

Figure 2 A plot of S/S_{Al} in y-direction at $x = 50$ μm in the sample (AA2024) from Fig. 1 shows the typical statistical error. The line is just a guide for the eye.

3.3. Plastic zone in AA2024 deformed in a corrosive medium

Compared to AA2024 samples deformed in air, the plastic zone in front of a crack tip generated in a corrosive environment shows a larger spatial extension which changes significantly at RT storage.

The plastic zone of AA2024 in NaCl has an extension of 200 μm $\times$ 250 μm and shows a maximum S/S_{Al}-value of 1.018 ± 0.003 (Fig. 3a, measured instantly after crack generation). After storing the sample for two weeks at RT in the laboratory the size of the plastic zone has decreased to 100 μm $\times$ 200 μm while the maximum S/S_{Al}-value dropped 1.011 ± 0.002 (Fig. 3b).

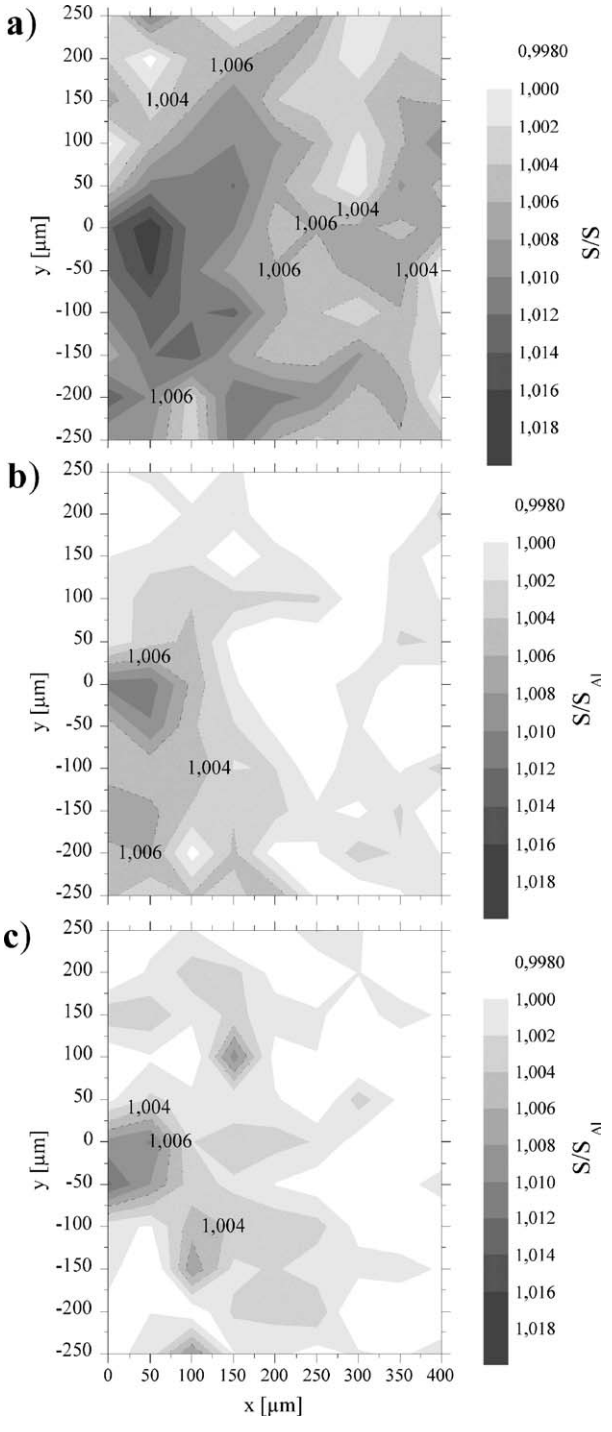

Figure 3 Changes of the plastic zone in AA2024 produced in corrosive solution over time at RT: (a) instantly, (b) two weeks, and (c) six weeks after crack creation.

After four more weeks storage at RT the plastic zone is reduced to an extension of 100 μm $\times$ 100 μm exhibiting a maximum S/S_{Al}-value of 1.012 ± 0.002 (Fig. 3c). This behaviour has never been observed after deformation in air.

3.4. Plastic zone in AA6013 deformed in air

The region in front of the crack tip in the aluminium alloy 6013 deformed in air looks similar to the plastic zone in AA2024 deformed in air. The only difference between them is its smaller extension. In AA6013 the plastic zone has a size of 100 μm $\times$ 75 μm with a maximum S/S_{Al}-value of 1.044 ± 0.003 (Fig. 4). Here the border of the plastic zone is set at $S/S_{Al} = 1.036$. As in the case of AA2024, the dimension of the plastic zone remains constant over the time of several weeks.

Fig. 5 shows a line scan at $x = 50$ μm as an example for the statistical error distribution. The solid line is a guide for the eye.

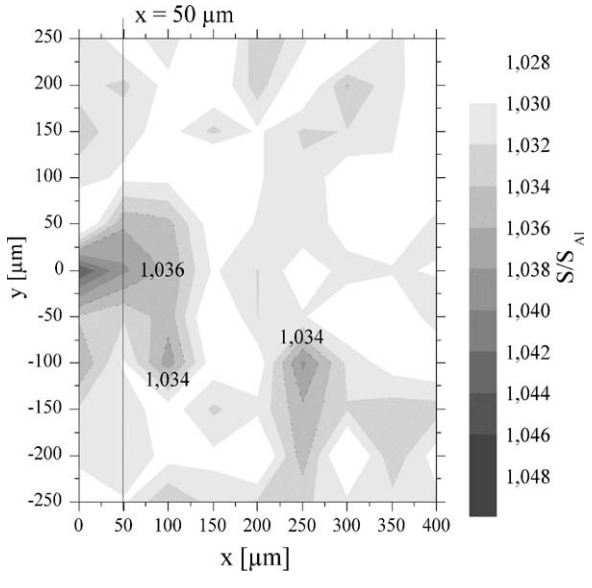

Figure 4 Plastic zone in front of the crack tip in AA6013 deformed in air. The solid line shows the position of the line scan in Fig. 5.

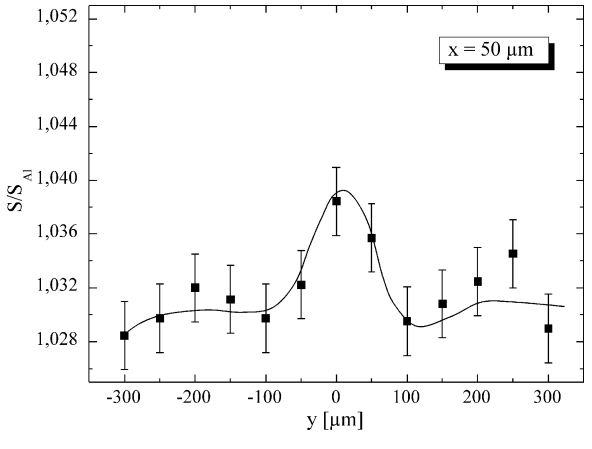

Figure 5 A plot of S/S_{Al} in y-direction at $x = 50$ μm in the same sample (AA6013) shows the typical statistic error. The line is just a guide for the eye.

3.5. Plastic zone in AA6013 deformed under corrosive conditions

Under the influence of the corrosive environment during crack generation the size of the deformed region as well as the observed maximum S/S_{Al}-value both increase. The extension of the plastic zone measured instantly after crack creation is determined to be 150 μm $\times$ 200 μm having a maximum S/S_{Al}-value of 1.049 ± 0.003 (Fig. 6a).

After storing the sample for three weeks at RT the size of the plastic zone is reduced to 100 μm $\times$ 200 μm while the maximum of the S/S_{Al}-value drops to 1.047 ± 0.003 (Fig. 6b). After nine weeks at RT a

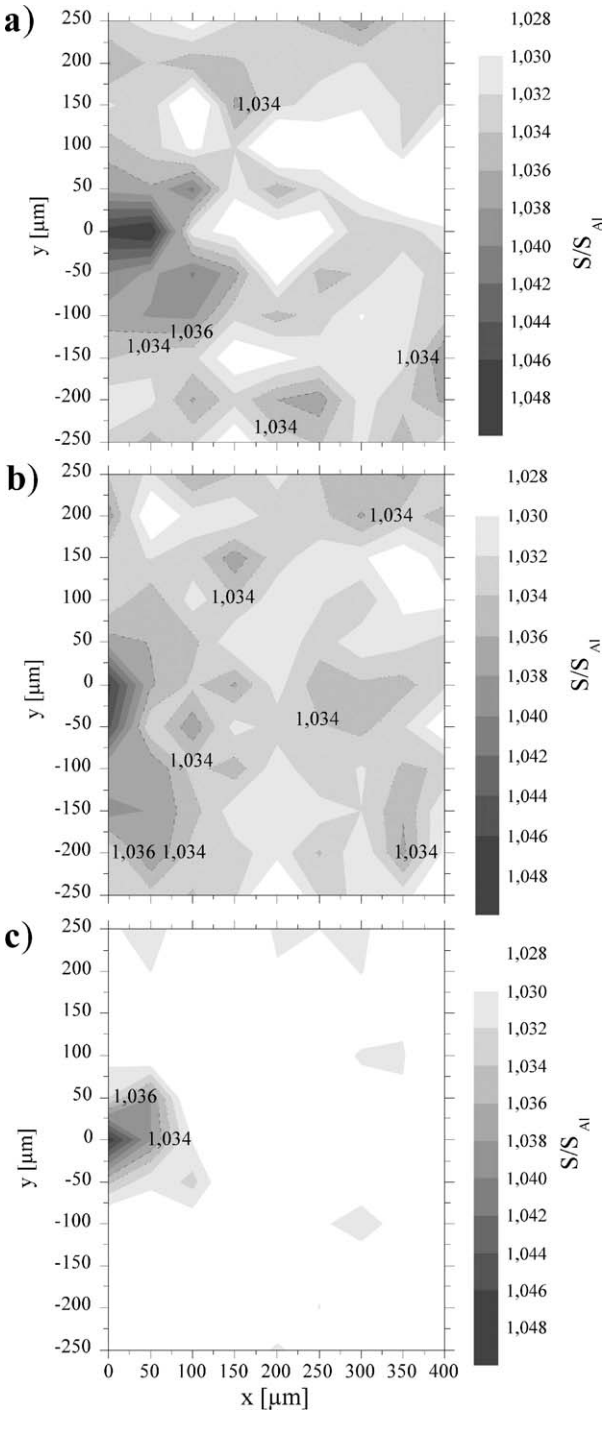

Figure 6 Changes of the plastic zone in AA6013 generated in corrosive solution over time at RT: (a) instantly, (b) three weeks, and (c) nine weeks after crack generation.

plastic zone of 100 μm $\times$ 200 μm remains which is comparable to the size of the plastic zone created in air while the maximum S/S_{Al}-value is still high: 1.047 ± 0.002 (Fig. 6c).

4. Discussion

During the fatigue fracture process a fresh active metallic surface is created at the crack tip site. In air, this surface is passivated immediately by oxidation to Al_2O_3. Exposed to the corrosive medium, the Al at the surface will dissolve to either form $Al(OH)_2^+$ or $Al(OH)_3$ depending on the pH-value and the Cl^- concentration of the environment [5]. In both redox reactions H_3O^+ ions are produced at the surface, which then dissociate to H_2O and H^+. At the test frequency of 1 Hz, the wetting of the active surface with the solution is guaranteed. Hence, the protons are in direct contact with the fresh fracture surface from which they obtain electrons to form atomic hydrogen. Diffusion of hydrogen into the metal then occurs. In Al alloys, hydrogen is highly mobile at RT in the interstitial lattice and can be trapped to open volume defects like vacancies and dislocations. This is due to the well known macroscopic effect that the solubility of hydrogen in deformed metals is larger than in annealed ones.

In a Vacancy, the trapping site for a hydrogen atom is not located in the geometric centre but in the vicinity of the surrounding metal atoms due to the short bond length H-Al [22]. Hence, the open volume is not masked for PAS by low concentrations of hydrogen, as numerical simulations and positron lifetime measurements have shown [23]. The migration energy of interstitial hydrogen in Al has been found to be 0.42 eV corresponding to a high mobility for temperatures above 100 K. The dissociation energy of a hydrogen vacancy complex is 0.95 ± 0.03 eV, which is related to a dissociation temperature of 295 ± 10 K [24, 25].

Due to the dissociation energy of the hydrogen vacancy complex, the annealing of vacancies is shifted from 220 K in hydrogen free aluminium [26, 27] to higher temperatures. Thus the vacancy concentration instantly after the deformation process is increased. Therefore, directly after crack production in both alloys in corrosive solution plastic zones larger than after deformation in air are detected by PAS measurements (see Table II).

TABLE II S/S_{Al}-values and size of plastic zones in AA2024 and AA6013

	S_{Bulk}/S_{Al}	Size of plastic zone (μm^2)	S_{max}/S_{Al}
2024 in air	1.001	125 $\times$ 175	1.017
2024 in NaCl	1.001	200 $\times$ 250	1.018
2024 in NaCl after 2 weeks	1.001	100 $\times$ 200	1.011
2024 in NaCl after 6 weeks	1.001	100 $\times$ 100	1.012
6013 in air	1.025	100 $\times$ 75	1.044
6013 in NaCl	1.025	150 $\times$ 200	1.049
6013 in NaCl after 3 weeks	1.025	100 $\times$ 200	1.047
6013 in NaCl after 9 weeks	1.025	100 $\times$ 200	1.047

As shown in Figs 3 and 6, we observe experimentally a size reduction of the plastic zone occurring at RT with a time constant of roughly several weeks for AA2024 and AA6013, respectively (see also Table II). This seems to be related to the annealing of vacancy-hydrogen complexes.

Generally, the crack propagation rate in corrosive media is increased due to the corrosive environment. This effect is more pronounced for AA6013 than for AA2024. Qualitatively, both alloys show hydrogen diffusion into the metal from the sodium chloride solution, where the effect is quantitatively stronger for AA2024. In contrast to hydrogen embrittlement in ferritic steel, the hydrogen diffusion to the stress fields around the precipitations leads to an increased ductility and, hence, to additional energy absorption. Recent an-elastic measurements at crack tips in these materials strongly support this interpretation [28]. This effect is counteracting the cracking due to corrosive environment and partly balancing its detrimental influence.

5. Conclusion

Fatigue cracks in the alloys AA2024 and AA6013 were produced at RT in air and in corrosive solution. The plastic zone in front of the crack tip was observed with laterally resolved positron annihilation spectroscopy in the micron range using the Bonn Positron Microprobe. Due to the presence of vacancies as well as dislocations the positron annihilation signal leads to a higher S-parameter. For both alloys, the plastic zone observed after a crack generation in a corrosive medium is larger than the corresponding one after crack generation in air. In AA2024, this effect is more pronounced than in AA6013. According to the general understanding of plasticity, this indication of increased ductility leads to a decelerated crack growth rate in AA2024 compared to AA6013—both in corrosive medium. The effect of the larger plastic zone partly compensates the otherwise negative effect of generally increased crack propagation in the corrosive medium. The discovered enlargement of the plastic zones disappears within several weeks provided that the samples of both alloys are stored at room temperature exposed to normal air moisture. We attribute this to an increased concentration of hydrogen in the plastic zone, which may become trapped at vacancies. Therefore, the effective vacancy migration energy is increased.

References

1. A. WILM, *Metallurgie* **8** (1911) 225.
2. R. P. WEI and J. D. LANDES, *Mater. Res. Stand* **9** (1969) 25.
3. I. TOCKELS, G. LÜTJERING and A. GYSLER, *Mater. Sci. Forum* **217** (1996) 1599.
4. K. NOCKE, F. BERGNER, H. BERSCH, I. HAASE, H. WORCH, G. TEMPUS and E. LOECHELT, *Mater. Corros.* **51** (2000) 628.
5. I. HAASE, K. NOCKE, H. WORCH, G. ZOUHAR and G. TEMPUS, *Prakt. Metallogr.* **38** (2001) 3, 119.
6. H.-J. SCHMIDT and BRANDECKER, in "Fatigue '96" (Elsevier Science, Oxford, UK, 1996) p. 643.
7. D. S. DUGDALE, *J. Mech. Phys. Soc.* **8** (1960) 100.

8. I. K. MACKENZIE, T. L. KHOO, A. B. McDONALD and B. T. A. MCKEE, *Phys. Rev. Lett.* **19** (1967) 946.
9. R. KRAUSE-REHBERG and H. S. LEIPNER, "Positron Annihilation in Semiconductors" (Springer Verlag, Berlin Heidelberg, 1999).
10. H. GREIF, M. HAAKS, U. HOLZWARTH, U. MÄNNIG, *et al.*, *Appl. Phys. Lett.* **71** (1997) 2115.
11. R. W. BALUFFI, *J. Nucl. Mater.* **69/70** (1978) 240.
12. B. THANABOONSOMBUT and T. H. SANDERS, The 4th International Conference on Aluminium Alloys (1994) p. 197.
13. Y. A. BAGARYATSKY, *Dokl. Akad. Nauk SSSR* **87** (1952) 397.
14. T. WIDER, S. HANSEN, U. HOLZWARTH and K. MAIER, *Phys. Rev.* B **57**(9) (1998) 512C.
15. M. HAAKS, K. BENNEWITZ, H. BIHR, U. MÄNNIG, C. ZAMPONI and K. MAIER, *Appl. Surf. Sci.* **149** (1999) 207.
16. R. N. WEST, *Adv. Phys.* **22** (1973) 263.
17. P. J. SCHULTZ and K. G. LYNN, *Rev. Mod. Phys.* **60**(3) (1988) 701.
18. M. J. PUSKA and R. M. NIEMINIEN, *ibid.* **66** (1994) 841.
19. G. DLUBEK, O. BRÜMMER, J. YLI-KAUPPILA and P. HAUTOJÄRVI, *J. Phys. F: Metal Phys.* **11** (1981) 2525.
20. A. DUPASQUIER, P. FOLEGATI, N. DE DIEGO and A. SOMOZA, *J. Conds. Matter* **10** (1998) 10409.
21. T. E. M. STAAB, E. ZSCHECH and R. KRAUSE-REHBERG, *J. Mater. Sci.* **35** (2000) 4667.
22. H. HJELMBERG, *Surf. Sci.* **81** (1979) 539.
23. H. E. HANSEN, R. M. NIEMINEN and M. J. PUSKA, *J. Phys. F: Met. Phys.* **14** (1984) 1299.
24. W. EICHENAUER, K. HATTENBACH and A. PEBLER, *Z. Metallkd.* **52** (1961) 682.
25. S. LINDEROTH, H. RAJAINMÄKI and R. M. NIEMINEN, *Phys. Rev. B* **35**(11) (1986) 5524.
26. W. WAMPLER and W. GAUSTER, *J. Phys. F* **8** (1978) 310.
27. F. PLEITER and C. HOHENEMSER, *Phys. Rev.* B **25** (1982) 106.
28. S. SONNEBERGER, Diploma Thesis, University Bonn, Germany, 2002.

Received 11 November 2003
and accepted 23 June 2004